Acta Mechanica Solida Sinica, Vol. 20, No. 3, September, 2007 ISSN 0894-9166
Published by AMSS Press, Wuhan, China. DOI: 10.1007/s10338-007-0728-7

CRACK PROPAGATION IN STRUCTURES SUBJECTED TO PERIODIC EXCITATION ⋆

Zhang Yin
(*State Key Laboratory of Nonlinear Mechanics* (*LNM*), *Institute of Mechanics, Chinese Academy of Sciences, Beijing* 100080, *China*)

Murphy Kevin D.
(*Department of Mechanical Engineering, University of Connecticut, CT* 06269-3139, *USA*)

Received 12 September 2006; revision received 23 August 2007

ABSTRACT In the present paper, a simple mechanical model is developed to predict the dynamic response of a cracked structure subjected to periodic excitation, which has been used to identify the physical mechanisms in leading the growth or arrest of cracking. The structure under consideration consists of a beam with a crack along the axis, and thus, the crack may open in Mode I and in the axial direction propagate when the beam vibrates. In this paper, the system is modeled as a cantilever beam lying on a partial elastic foundation, where the portion of the beam on the foundation represents the intact portion of the beam. Modal analysis is employed to obtain a closed form solution for the structural response. Crack propagation is studied by allowing the elastic foundation to shorten (mimicking crack growth) if a displacement criterion, based on the material toughness, is met. As the crack propagates, the structural model is updated using the new foundation length and the response continues. From this work, two mechanisms for crack arrest are identified. It is also shown that the crack propagation is strongly influenced by the transient response of the structure.

KEY WORDS crack propagation/arrest, elastic foundation, modal analysis, vibration, natural frequency

I. INTRODUCTION

For structures possessing a crack (or delamination in a layered medium), numerous criteria have been put forth predicting (i) whether crack growth will be initiated and (ii) how that growth proceeds, for example, the review by Shukla[1]. And while some have examined how the wave propagation characteristics of the system (which transmits the stress induced by a remote, impulsive load) influence crack growth, there are relatively few authors that have examined how the overall structural response can influence this phenomenon. One such structural model was suggested by Dowell[2], which consists of a cantilever beam of thickness $2h$ with an end crack parallel to the x-axis, as shown in Fig.1(a). A couple of external loads are applied at the right edge of the cracked beam. Because of the symmetry about the midplane, this system can be modeled as a single beam of thickness h resting on a partial elastic foundation, see Fig.1(b). The portion of the beam on the foundation represents the intact portion of the structure. Dowell predicted the static parameter combinations that would lead to crack propaga-

⋆ Zhang is supported by the National Natural Science Foundation of China (NSFC, Grant No.10502050). Murphy is supported by the National Science Foundation (Grant No.0085122) of the United States of America.

tion; this propagation is mimicked by allowing the lead spring in the foundation (i.e., the crack tip) to break — thereby shrinking the foundation size d. The benefits of this model are twofold. First, it is not a mathematically complex model — making it accessible for undergraduates. Second, it provides useful trends regarding parameter combinations that lead to propagation. Moreover, these trends are explained in the fundamental physics of the system. Finally, it is also worth mentioning that, while this model was originally developed to examine crack growth, it can easily be extended to address problems of delamination in composites[3], adhesion and de-adhesion in microelectromechanical systems[4–6].

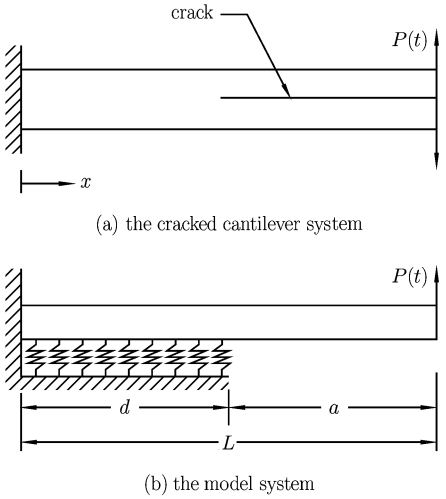

Fig. 1 A schematic of the system.

The present paper extends the Dowell model by including dynamic effects. For a given foundation length, the natural frequencies and mode shapes are found from the free vibration eigenvalue problem. Then the modal analysis is used to find the total response for a periodic excitation $P(t)$. Crack propagation is initiated if the lateral displacement at the crack tip exceeds a critical value that is obtained from the stress intensity factor. Once the foundation shrinks, the natural frequencies and mode shapes are recalculated and the model is updated. Of course, this has the effect of inducing further transients in the response. This process continues until either the system settles into a steady state (such that the crack growth is arrested) or the crack runs the length of the structure.

The dynamic response is calculated for a set of parameters and instances of crack propagation and crack arrest are clearly demonstrated. Three physical mechanisms are proposed to explain the various behaviors seen. These involve (i) the change in the natural frequencies, (ii) the influence of structural nodes, and (iii) transient effects. Finally, a diagram showing excitation parameter combinations leading to unstable crack growth is developed. This highlights the importance of the third mechanism.

II. MODEL DEVELOPMENT

2.1. Equation of Motion

Figure 1(b) shows a schematic of the cantilevered beam resting on a partial elastic foundation. The crack has length a and the intact portion of the beam has length d. The beam length is L. The equation of motion is found using Hamilton's principle, $\delta \int_{t_1}^{t_2}(T-U+W)\mathrm{d}t = 0$, where T is the kinetic energy, U is the strain energy, and W is the external work. The kinetic energy is

$$T = \frac{m}{2}\int_0^L (w_{,t})^2 \mathrm{d}x \tag{1}$$

where $m = \rho bh$ is the mass per unit length with ρ denoting the density, b and h being the width and thickness of the beam cross section, respectively. $w(x,t)$ is the transverse displacement, and $(\circ)_{,t} \equiv \partial(\circ)/\partial t$. The strain energy for a linear elastic beam resting on a partial linear elastic foundation of length d is

$$U = \frac{EI}{2}\int_0^L (w_{,xx})^2 \mathrm{d}x + \frac{k}{2}\int_0^L [1-H(x-d)]w^2 \mathrm{d}x \tag{2}$$

where E and I are the elastic modulus and the area moment of inertia, respectively. $I = bh^3/12$ for a rectangular cross section. $w_{,xx} = \partial^2 w/\partial x^2$ and k is the elastic foundation modulus. $H(x)$ is the Heaviside function. External work done by the applied load $P(t)$ is:

$$W = \int_0^L P(t)w(x,t)\delta(x-x_o)\mathrm{d}x = P(t)w(x_o,t) \tag{3}$$

where $\delta(x)$ is the Dirac delta function and x_o is the load location ($x_o = L$ in Fig.1).

Applying Hamilton's principle and carrying out the necessary integration by parts leads to the following equation of motion

$$mw_{,tt} + EIw_{,xxxx} + k[1 - H(x-d)]w = P(t)\delta(x - x_o) \tag{4}$$

For convenience in use, the displacement field is written as the following two parts:

$$w(x,t) = \begin{cases} w_1(x,t) & (0 \le x < d) \\ w_2(x,t) & (d \le x \le L) \end{cases} \tag{5}$$

This reduces the equation of motion to two equations whose solutions must satisfy certain matching conditions at $x = d$. Thus, the free vibration of the system can be expressed by the following two equations

$$mw_{1,tt} + EIw_{1,xxxx} + kw_1 = 0 \qquad (0 \le x < d) \tag{6}$$

and

$$mw_{2,tt} + EIw_{2,xxxx} = 0 \qquad (d \le x \le L) \tag{7}$$

The eight boundary/matching conditions are derived from the Hamilton's principle as follows:

$$\begin{array}{llll} w_1(0) = 0, & w_{1,x}(0) = 0, & w_{,xx}(L) = 0, & w_{2,xxx}(L) = 0 \\ w_1(d) = w_2(d), & w_{1,x}(d) = w_{2,x}(d), & w_{1,xx}(d) = w_{2,xx}(d), & w_{1,xxx}(d) = w_{2,xxx}(d) \end{array} \tag{8}$$

Obviously, the two displacement fields w_1 and w_2 are coupled with each other through the matching conditions at $x = d$.

2.2. Natural Frequencies and Mode Shapes

The free vibration solution begins by assuming w_1 and w_2 as the harmonic motion: $w_1 = \psi^{\mathrm{I}}(x)\mathrm{e}^{\mathrm{i}\Omega t}$ and $w_2 = \psi^{\mathrm{II}}(x)\mathrm{e}^{\mathrm{i}\Omega t}$. Substitution of these expressions into Eqs.(6) and (7) leads to the following two fourth order differential equations for the functions ψ^{I} and ψ^{II}:

$$\psi^{\mathrm{I}}_{,xxxx} - \frac{m\Omega^2 - k}{EI}\psi^{\mathrm{I}} = 0 \qquad (0 \le x < d) \tag{9}$$

$$\psi^{\mathrm{II}}_{,xxxx} - \frac{m\Omega^2}{EI}\psi^{\mathrm{II}} = 0 \qquad (d \le x \le L) \tag{10}$$

Ω is the natural frequency, which will be determined by the boundary/matching conditions. Before determining Ω, the solution form for ψ^{I} and ψ^{II} requires a careful discussion. The solution for ψ^{II} follows the standard beam solution. However, there are three possible solution forms for ψ^{I} depending on the value of $\dfrac{m\Omega^2 - k}{EI}$.

∗ **Case 1:** $\dfrac{m\Omega^2 - k}{EI} > 0$. In this case, the wave number is real and the mode is said to be cut-on[7]. The eigen-function is

$$\psi^{\mathrm{I}}(x) = A_1 \sin(\lambda_1 x) + A_2 \cos(\lambda_1 x) + A_3 \sinh(\lambda_1 x) + A_4 \cosh(\lambda_1 x) \tag{11}$$

where $\lambda_1^4 = \left|\dfrac{m\Omega^2 - k}{EI}\right|$.

∗ **Case 2:** $\dfrac{m\Omega^2 - k}{EI} < 0$. The wave number is complex and the eigen-function is

$$\psi^{\mathrm{I}}(x) = A_1\mathrm{e}^{\alpha x}\cos(\alpha x) + A_2\mathrm{e}^{\alpha x}\sin(\alpha x) + A_3\mathrm{e}^{-\alpha x}\cos(\alpha x) + A_4\mathrm{e}^{-\alpha x}\sin(\alpha x) \tag{12}$$

with $\alpha = \dfrac{\sqrt{2}}{2}\sqrt[4]{\dfrac{k - m\Omega^2}{EI}}$. This solution can be shown in Appendix I that it can not be a solution form of a finite beam on an elastic foundation. But it is a solution form for an infinite beam on an elastic foundation as discussed by Graff[7]. Timoshenko, Young and Weaver[8] take only cut-on frequency solution form (Case 1) without a proof for the solution of a finite beam on an elastic foundation. Appendix I gives a detailed proof.

∗ **Case 3:** $\dfrac{m\Omega^2 - k}{EI} = 0$. The mode shape ψ^{I} has the solution form

$$\psi^{\mathrm{I}}(x) = A_1 x^3 + A_2 x^2 + A_3 x + A_4 \tag{13}$$

The eigenfrequency solved from this form of solution is called cut-off frequency. The cut-off frequency, as pointed out by Perkins[9] is always the solution for a characteristic equation. It is shown in Appendix I that the above polynomial form of mode shape can only be linear (i.e., $A_1 = A_2 = 0$), which is only possible under rigid body motion.

ψ^{II} has the following expression

$$\psi^{\mathrm{II}} = B_1 \sin(\lambda_2 x) + B_2 \cos(\lambda_2 x) + B_3 \sinh(\lambda_2 x) + B_4 \cosh(\lambda_2 x) \tag{14}$$

where $\lambda_2^4 = \dfrac{m\Omega^2}{EI}$. Using Eq.(11) for ψ^{I} and Eq.(14) for ψ^{II}, the eight boundary/matching conditions of Eq.(8) are applied. This produces eight simultaneous algebraic equations. For nontrivial solutions, the determinant is required to be zero. This leads to the following characteristic equation

$$\begin{vmatrix}
0 & 1 & 0 & 1 & 0 & 0 & 0 & 0 \\
1 & 0 & 1 & 0 & 0 & 0 & 0 & 0 \\
\sin(\lambda_1 d) & \cos(\lambda_1 d) & \sinh(\lambda_1 d) & \cosh(\lambda_1 d) & -\sin(\lambda_2 d) & -\cos(\lambda_2 d) & -\sinh(\lambda_2 d) & -\cosh(\lambda_2 d) \\
\lambda_1 \cos(\lambda_1 d) & -\lambda_1 \sin(\lambda_1 d) & \lambda_1 \cosh(\lambda_1 d) & \lambda_1 \sinh(\lambda_1 d) & -\lambda_2 \cos(\lambda_2 d) & \lambda_2 \sin(\lambda_2 d) & -\lambda_2 \cosh(\lambda_2 d) & -\lambda_2 \sinh(\lambda_2 d) \\
-\lambda_1^2 \sin(\lambda_1 d) & -\lambda_1^2 \cos(\lambda_1 d) & \lambda_1^2 \sinh(\lambda_1 d) & \lambda_1^2 \cosh(\lambda_1 d) & \lambda_2^2 \sin(\lambda_2 d) & \lambda_2^2 \cos(\lambda_2 d) & -\lambda_2^2 \sinh(\lambda_2 d) & -\lambda_2^2 \cosh(\lambda_2 d) \\
-\lambda_1^3 \cos(\lambda_1 d) & \lambda_1^3 \sin(\lambda_1 d) & \lambda_1^3 \cosh(\lambda_1 d) & \lambda_1^3 \sinh(\lambda_1 d) & \lambda_2^3 \cos(\lambda_2 d) & -\lambda_2^3 \sin(\lambda_2 d) & -\lambda_2^3 \cosh(\lambda_2 d) & -\lambda_2^3 \sinh(\lambda_2 d) \\
0 & 0 & 0 & 0 & -\lambda_2^2 \sin(\lambda_2 L) & -\lambda_2^2 \cos(\lambda_2 L) & \lambda_2^2 \sinh(\lambda_2 L) & \lambda_2^2 \cosh(\lambda_2 L) \\
0 & 0 & 0 & 0 & -{\lambda_2}^3 \cos(\lambda_2 L) & \lambda_2^3 \sin(\lambda_2 L) & \lambda_2^3 \cosh(\lambda_2 L) & \lambda_2^3 \sinh(\lambda_2 L)
\end{vmatrix} = 0 \tag{15}$$

The natural frequencies Ω are obtained by numerically root solving the above characteristic equation. Once the frequencies are obtained, the eigenfunctions are also specified; the mode shape for the entire beam is written as a composite of the two functions ψ^{I} and ψ^{II}, namely, $\psi = \psi^{\mathrm{I}} + H(x-d)(\psi^{\mathrm{II}} - \psi^{\mathrm{I}})$.

Orthogonality is very important here, which allows us to decouple the equation in using the Galerkin method. The orthogonality property of mode shape ψ is proved in Appendix II.

2.3. Modal Analysis

If proportional damping is added to the system, the equation of motion becomes

$$m w_{,tt} + c w_{,t} + EI w_{,xxxx} + k[1 - H(x-d)]w = P_o \sin(\omega t)\delta(x - L) \tag{16}$$

where c is the damping coefficient. As the interfacial debonding is accompanied with dissipation of interface adhesion energy[10], a damping term as above should be introduced to model such dissipation. P_o and ω are the amplitude and the driving frequency of the external excitation force, respectively. The external excitation force is acted at the free end (i.e. $x_o = L$). To solve this equation, an expansion of the form $w(x,t) = \sum_{j=1}^{N} \phi_j(t)\psi_j(x)$ is assumed, where $\phi_i(t)$'s are the unknown, time-dependent modal amplitudes. Substituting this into the equation of motion and using the orthogonality condition of the modes results in the following equation governing the j-th modal amplitude (See Appendix III for the derivation in detail):

$$\ddot{\phi_j} + 2\xi_j \Omega_j \dot{\phi_j} + \Omega_j^2 \phi_j = \frac{P_o \sin(\omega t)\psi^{\mathrm{II}}(L)}{m \int_0^L \psi_j^2 \mathrm{d}x} = f_j \sin(\omega t) \tag{17}$$

where $\xi_j = c/(2m\Omega_j)$ and Ω_j is the j-th eigenfrequency computed from the characteristic equation of Eq.(15). It needs to be emphasized that the repeated subscript j in above Eq.(17) does not mean summation. The overdot refers to differentiation with respect to time. The solution of ϕ_j is

$$\phi_j = \mathrm{e}^{-\xi_j \Omega_j t}[A_j \sin(\sqrt{1-\xi^2}\Omega_j t) + B_j \cos(\sqrt{1-\xi^2}\Omega_j t)] + E_j \sin(\omega t) + F_j \cos(\omega t) \tag{18}$$

A_j, B_j, E_j and F_j are the constants determined by the initial conditions and external excitation force. The first two terms associated with A_j and B_j are the transient motion and the last two associated with E_j and F_j are the steady state motion. c is taken as $c = 40$ Pa·s, which sets $\xi_1 = 0.1$ of an underdamped case.

2.4. A Criterion for Dynamic Crack Growth

In the above, a model for the lateral deflection of a cracked beam has been presented. In keeping with this approach, it is desirable to have a crack growth criterion (signaling the onset of crack propagation) expressed in terms of the lateral deflection at the crack tip, $w(d,t)$. In contrast with the static fracture toughness, determining dynamic fracture toughness is a difficult issue[11]. Tremendous efforts have been made to study the dynamic crack growth[1, 11–20]. Various criteria have been proposed previously, which include using displacement quantities such as the crack gradient profile, the normal crack opening displacement, or the vectorial crack-face displacement to predict crack growth[12–15] and others like energy criteria[10]. In the present study, the stress intensity factor is related to the lateral displacement at the crack tip. By using this relation, the material toughness (a critical value of the stress intensity factor associated with the onset of crack growth) is then used to find a critical crack tip displacement, $w_{\rm cr}$, once $w(d,t) \geq w_{\rm cr}$, the crack is permitted to grow. The toughness used here is a static one, which can be significantly larger than a dynamic one due to the dynamic/inertial effect[12, 18, 19]. Unlike those impulse/pulse loadings[16–19], the external excitation force used here is a periodically shaking force with a relatively low frequency. From the analysis of Freund[12] and experiments of Shockey et al.[18, 19], it is suitable to assume the dynamic toughness is the same as the static one when the loading is not very fast and crack growth speed is low. In the calculation[21] the beam material is chosen as steel with $E = 2 \times 10^{12}$ Pa and $K_{\rm IC} = 4 \times 10^7$ Nm$^{-3/2}$. Obviously, steel is not a brittle material and crack growth can not be fast. For the model in this paper or others which also uses the displacement as the variable[22], choosing the displacement as the crack growth criterion or say, translating the toughness criterion into a displacement one makes the problem straightforward.

To explain how the critical crack tip displacement $w_{\rm cr}$ is obtained, let's begin by considering the stress intensity factor for the double cantilever beam model[23]

$$K_{\rm I} = \frac{2\sqrt{3}Pa}{bh^{3/2}} \tag{19}$$

where P is a constant load applied at the beam tip, a is the crack length and b, h are the width and thickness of the beam, respectively. A critical load (to initiate crack propagation) may be obtained by substituting the toughness $K_{\rm IC}$ for the stress intensity factor: $P_{\rm cr} = \dfrac{K_{\rm IC}bh^{3/2}}{2\sqrt{3}a}$. This is the critical static force required to initiate crack growth. By using this load, the lateral displacement at the crack tip $w(d,t)$ may be found by the following procedures of statics. For statics, Eq.(16) now becomes

$$EIw_{,xxxx} + k[1 - H(x-d)]w = P_{\rm cr}\delta(x-L) \tag{20}$$

$P_o \sin(\omega t)$ in Eq.(16) is substituted by $P_{\rm cr}$. Assume the static displacement $w_s(x) = \sum\limits_{j=1}^{N} a_j\psi_j(x)$, a_j is the constant modal amplitude to be determined. The following equation is obtained by the same procedures of deriving Eq.(17)

$$\Omega_j^2 a_j = \frac{P_{\rm cr}\psi^{\rm II}(L)}{m\int_0^L \psi_j^2 {\rm d}x} \tag{21}$$

Therefore $a_j = \dfrac{P_{\rm cr}\psi^{\rm II}(L)}{(m\Omega_j^2 \int_0^L \psi_j^2 {\rm d}x)}$ and $w_{\rm cr} = w_s(d) = \sum\limits_{j=1}^{N} a_j\psi_j(d)$. For this study, $w_{\rm cr}$ (solved from the statics) is presumed to be the critical lateral crack tip displacement. Once $w(d,t) = w_{\rm cr}$, the crack begins to propagate until the tip reaches some new location $x = d$ where $w(d,t) < w_{\rm cr}$. It should be noted that, as the crack propagates, the value of $w_{\rm cr}$ changes because the free length of the beam has increased. This is described more completely in §3.1.

III. RESULTS AND DISCUSSION

3.1. A Mechanism for Unstable Crack Growth

It is well established in the fracture mechanics literature [12] that a specimen undergoing a constant load, as shown schematically in Fig.2(a), with $P \geq P_{\rm cr}$ will experience unstable crack growth, i.e., the crack will grow indefinitely. The physical reason for this is as follows: As the crack begins to grow, the

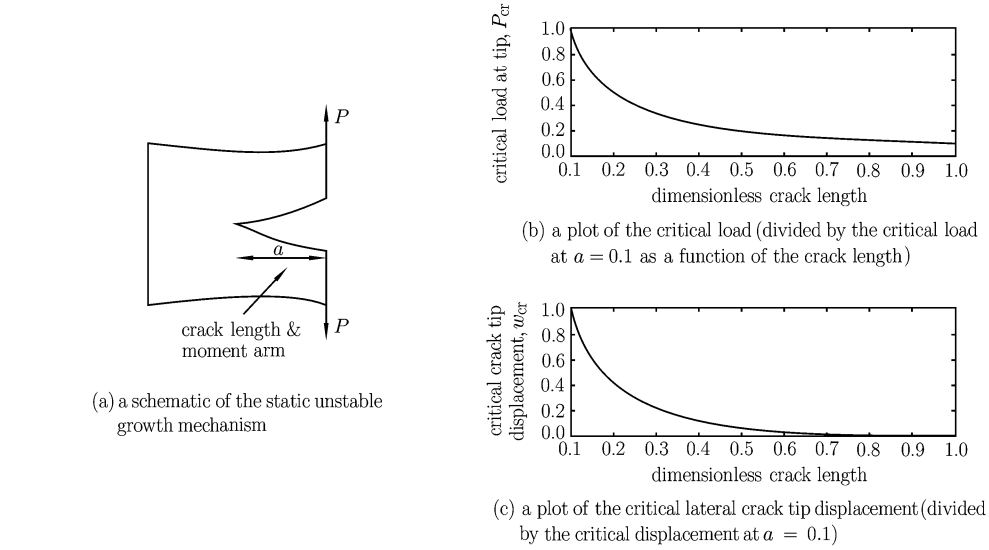

(a) a schematic of the static unstable growth mechanism

(b) a plot of the critical load (divided by the critical load at $a = 0.1$ as a function of the crack length)

(c) a plot of the critical lateral crack tip displacement (divided by the critical displacement at $a = 0.1$)

Fig. 2. The critical load and displacement at $a = 0.1$ m, $P_{\rm cr} = 3267.5$ N and $w_{\rm cr} = 6.454 \times 10^{-2}$ m.

moment arm extending from the crack tip to the load gets larger. The increased moment fuels the crack growth and the situation gets worse. Alternatively, this can be viewed from a mathematical perspective by noting that the critical load, $P_{\rm cr} = \dfrac{K_{\rm IC} b h^{3/2}}{2\sqrt{3}a}$ (from §2.4), is inversely proportional to the crack length. This is shown graphically in Fig.2(b), which indicates that as the crack grows the critical load diminishes. Hence, under a constant load, the crack propagation is unstable.

For the sake of this research, the crack growth criterion is described in terms of the lateral displacement of the crack tip, $w(d, t)$. Specifically, a critical crack tip displacement is found by using elementary statics to determine the crack tip displacement under the critical load, $P_{\rm cr}$. Since the critical load varies with the crack length, the critical crack tip displacement, $w_{\rm cr}$ is also dependent on crack length, as shown in Fig.2(c). Consequently, as the crack grows, the required lateral crack tip displacement to maintain crack growth decreases. And so, from a static perspective, the possibility of continued (unstable) crack growth becomes more likely. This is the fundamental mechanism for unstable crack growth in this system.

3.2. Model Validation

Prior to addressing all of the mechanisms at play in the crack growth problem, our first goal is to validate the behavior of the analytical model developed in §II of this paper. As a means of comparison, the finite element method (FEM) is used to discretize the model using one hundred beam elements. The

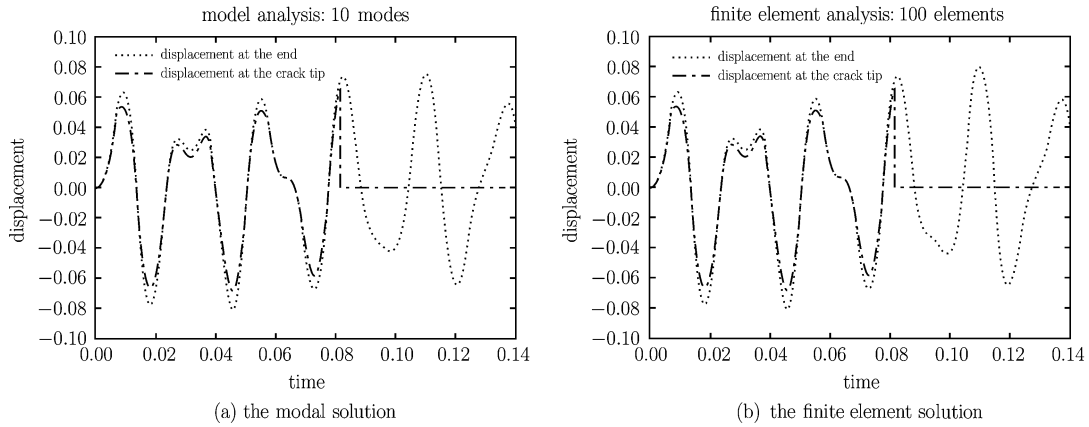

(a) the modal solution

(b) the finite element solution

Fig. 3. Motion of the beam tip and crack tip as determined by different solutions. $\omega = 645$ Hz and $P_o = 1600$ N.

FEM model is integrated using Hughes-Hilbert-Taylor (HHT) implicit integrator[24] and the same crack growth criterion is used. Though numerous test cases has been run, one typical result is shown in Fig.3 for the parameter combinations: $\omega = 645$ Hz, $P_o = 1600$ N, $kL^4/(EI) = 1.5$, and $a_{\text{initial}}/L = 0.1$. Here, the lateral displacement of the beam tip (at $x = L$) and the crack tip ($x = d$) are plotted as a function of time. In this paper, the following parameters are fixed: $E = 2 \times 10^{12}$ Pa, $K_{\text{IC}} = 4 \times 10^7$ Nm$^{-3/2}$ and $\rho = 4500$ kg/m^3 for steel; $L = 1$ m, $b = 0.01$ m and $h = 0.02$ m. The varying parameters are the external force amplitude P_o and frequency ω, elastic foundation modulus k and crack length a ($d = L - a$). Figure 3(a) is the result of analytical model and 3(b) is that of the finite element method. The results are strikingly similar and show that the system oscillates without crack propagation until approximately $t = 0.055$ sec. At that time crack propagation is initiated and the crack runs the entire length of the beam before it stops (signaling complete failure of the structure); the tip displacement simultaneously drops to zero. The mechanism for this unstable growth is outlined in §3.1. The quantitative agreement, observed in this simulation, confirms that the responses generated by the analytical modal analysis and FEM models represent consistent solutions to the governing equations.

3.3. Two Mechanisms for Crack Arrest

Two fundamental mechanisms for crack arrest are identified. Not surprisingly, both of these have to do with limiting the lateral displacement of the crack tip. The first mechanism has to do with the natural frequencies, which (in the undamped case) are also the resonant frequencies. To explore this, consider the influence of a crack of length a on the natural frequencies Ω_j of the system. This is shown in Fig.4. Figures 4(a) and (b) show the change in the first and the second natural frequencies, nondimensionalized by the no foundation frequency (Ω_j^{nf}, $j = 1$ and 2), as a function of crack length. Various foundation stiffnesses ($kL^4/(EI) = 1.5$, 20 and 50) are also shown. From these figures and from our intuition, it is evident that as the crack grows (and less of the foundation contacts the beam) the system de-stiffens and the frequencies drop. Asymptotically, these frequencies must approach the no foundation frequencies as $a/L \to 1$.

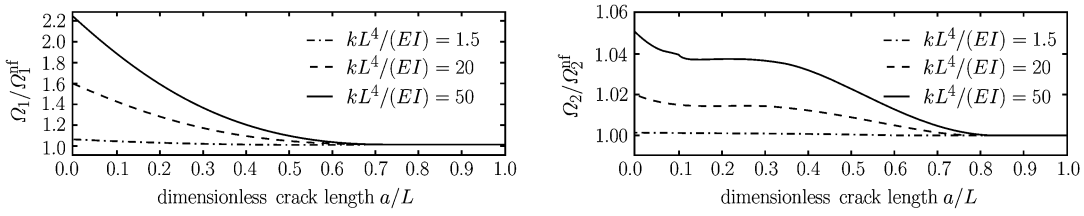

(a) the first natural frequency (b) the second natural frequency

Fig. 4. The change in the first two natural frequencies (normalized by the no foundation frequencies as a function of the crack length). Various foundation stiffness to bending stiffness ratios are shown. $\Omega_1^{\text{nf}} = 427.95$ Hz and $\Omega_2^{\text{nf}} = 2681.95$ Hz.

So how does this phenomenon affect crack growth? Consider the following: the system has a small crack (for example, $a/L = 0.1$) and is being driven at $\omega = \Omega_1$. In this case, large amplitude resonance will take place. These large oscillations can lead to sufficiently large lateral crack tip displacements to initiate crack growth (i.e., $|w(d,t)| \geq w_{\text{cr}}$). As the crack grows, the resonant frequency decreases, as shown in Fig.4(a). Provided the driving frequency doesn't change, the system is now 'off-resonance' and the magnitude of the crack tip amplitude will decrease. This reduction of amplitude at the crack tip may cause the crack propagation to cease.

The second mechanism for crack arrest stems from the modal aspect of the response. Consider our system with an initial crack length $a/L = 0.1$, which is being excited near its second natural frequency. The resonance will lead to sufficiently large lateral crack tip displacements to initiate crack growth. However, as the crack propagates to the left (see Fig.1), the crack tip will encounter a node in the vibration mode at approximately $x/L = 0.783447$. Since the vibration node has zero displacement, the crack tip is unable to travel through the node and the propagation is arrested. As an example of this arrest mechanism, consider a system with the following parameters: initial $d/L = 0.9$ ($a/L = 0.1$), $k = 2 \times 10^4$ Pa, $\omega = 2658$ Hz (close to $\Omega_2 = 2723.8$ Hz), $P_o = 900$ N. When all of the initial conditions

are set zero, the lateral response at the crack tip is shown in Fig.5(a). The associated longitudinal position of the crack tip is shown in Fig.5(b). For the entire time series shown, the response is clearly still in its transient phase but is dominated by the second mode. At $t \approx 0.0432$ sec the crack tip displacement exceeds the critical tip displacement and the lateral response jerks suddenly. What has happened to the crack tip (how far it has propagated) is unclear from the lateral response. However, two more such jerks are evident and labeled in Fig.5(a). The longitudinal movement of the crack tip at these same instances are clear in Fig.5(b). At $t \approx 0.0432$ sec, the crack tip suddenly runs from its initial location to $a/L = 0.16$, where it is temporarily arrested. As the system continues to vibrate, the crack tip propagates again to $a/L = 0.18$, where it is again arrested. A third propagation event occurs near $t = 0.06$ sec and the crack tip runs to $a/L = 0.20$ ($d/L = 0.80$). There is no further propagation and, eventually, the system settles down into a steady state oscillation. The physical reason that the crack arrested at $a/L = 0.20$ stems from the fact that the system is being driven near its second natural frequency; the crack has propagated close to the node in the vibration mode. Since the node has zero amplitude, the lateral crack tip displacement $w(d,t)$ must be less than $w_{\rm cr}$ and the propagation is completely arrested.

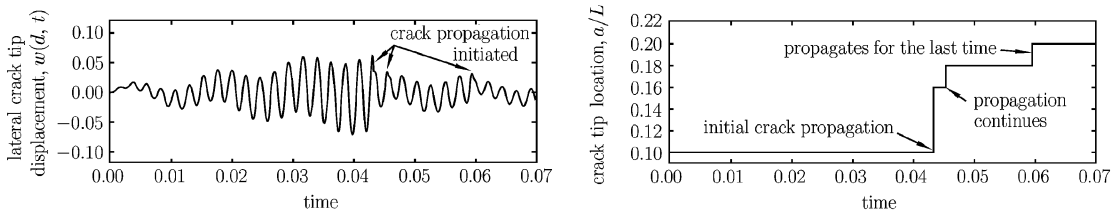

(a) The lateral response of crack tip (b) the horizontal motion of crack tip (crack propagation)

Fig. 5. Simulations showing the nodal arrest mechanisms. The driving frequency is around the second natural frequency.

3.4. The Role of Transients

In §3.1 and 3.3, mechanisms for crack growth and crack arrest have been offered. And the validity of these mechanisms is argued largely on the base of steady state phenomenon. Transient effects complicate this nice framework and tend to muddy the waters of our understanding. For example, the nodal arrest mechanism assumes that the crack tip will propagate to a node and then stop due to a lack of lateral motion at the node. And this can, in fact, occur (as highlighted by the example shown in Fig.5). However, this is not the whole story. As the crack propagates toward the node, additional transient oscillations are induced. The net/total motion, being the linear superposition of the transient and the steady state, may not have a small amplitude near the node. As such, the crack may not arrest. Similar arguments, undermining the crack growth and arrest mechanisms (§3.1 and 3.3), may be made.

To highlight the role of transient oscillations, a parameter study is undertaken. Figure 6 shows the excitation parameter combinations that will initiate crack propagation for the system parameters listed in §3.3, except that the driving frequency is near the first natural frequency. $a/L = 0.1$ and $k = 2 \times 10^4$ Pa in Fig.6. When $\omega = 0$, it is calculated as a static case and the critical load at the beam tip to initiate the crack growth is $P_{\rm cr} = 3267.5$ N. The solid line is generated using only the steady state solution. The circles are generated using the total solution (steady state + transient). Both cases agree that as the resonance is approached, the required forcing amplitude decreases due to the response amplification. How-

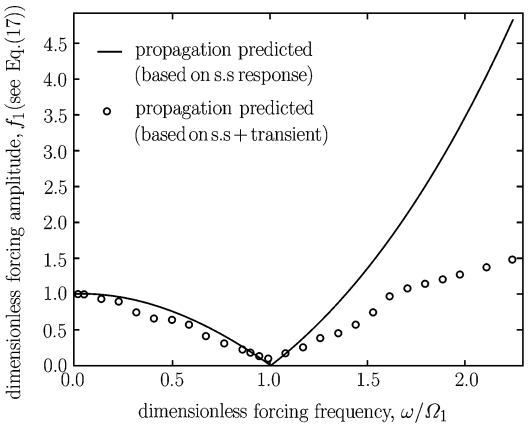

Fig. 6 Effects of transients-excitation parameters leading to crack growth. f_1 of the y-axis is the dimensionless force amplitude (see Eq.(17)) required to initiate the crack growth when the driving frequency is around the first natural frequency.

ever, it is revealing that above resonance the total response predicts the initiation of crack propagation at much lower forcing levels. This underscores the importance of the transient response in the initiation of crack growth.

IV. CONCLUSION

A very simple, yet powerful model is developed to capture the coupled dynamics of crack growth and structural vibration. The model consists of a cantilever beam attached to a linear elastic, partial foundation. The system is driven at the tip of the beam by a periodic load. And a solution to the governing equations is developed using classical modal analysis. The utility of this model stems from the fact that it mimics the behavior of a cracked, vibrating structure; the portion of the beam in contact with the elastic foundation is considered the intact portion of the structure. A crack growth criterion (based on the material toughness and the crack tip displacement) is also developed and used with the model; as the crack grows, the foundation length shrinks and the model must be updated.

This model is used to identify four key features related to the crack growth or crack arrest phenomenon. They are

• As the crack propagates (i.e., the foundation length shrinks), the required lateral crack tip displacement necessary to continue propagating the crack decreases. In this sense, propagation becomes easier with increased crack size/length.

• As the crack grows, the resonant frequencies drop. If the external driving frequency is at or above a resonance, this frequency shift (away from the driving frequency) decreases the response amplitude and reduces the likelihood of continued crack growth.

• If the system is driven at a higher resonant frequency, the appearance of a node in the response (associated with zero motion) can arrest crack growth.

• Transient effects can trump any of the aforementioned mechanisms. They can lead to crack growth (arrest) — even while one of the other mechanisms suggests the crack should arrest (grow).

These mechanisms can sometimes work with or against one another muddling our intuition as to whether crack growth will abate or continue. Regardless, the model developed herein provides some fundamental insight into the complex interaction between structural dynamics and the crack growth/arrest phenomenon.

References

[1] Shukla,A., High-speed fracture studies on bimaterial interfaces using photoelasticity-a review. *Journal of Strain Analysis*, 2001, 36(2): 119-142.

[2] Dowell,E.H., Crack extension in a double cantilevered beam model. *Journal of Applied Physics*, 1981, 52(8): 5356-5360.

[3] Gui,L. and Li,Z., Delamination buckling of stitched laminates. *Composites Science and Technology*, 2001, 61: 629-636.

[4] Jones,E.E., Begley,M.R. and Murphy,K.D., Adhesion of micro-cantilever subjected to mechanical point loading modeling and experiments. *Journal of the Mechanics and Physics of Solids*, 2003, 51: 1601-1622.

[5] Zhang,Y. and Zhao,Y.P., Static study of cantilever beam stiction under electrostatic force influence. *Acta Mechanica Solida Sinica*, 2004, 17: 104-112.

[6] Zhang,Y. and Zhao,Y.P., Vibration of an adhered microbeam under a periodically shaking electrical force. *Journal of Adhesion Science and Technology*, 2005, 19: 799-815.

[7] Graff,K.F., Wave Motion in Elastic Solids. Ohio State University Press, 1975.

[8] Timoshenko,S., Young,D.H. and Weaver,Jr.,W., Vibration Problems in Engineering, 4th Edition. John Wiley & Sons, 1974.

[9] Perkins,N.C., Linear dynamics of a translating string on an elastic foundation. *Journal of Vibration and Acoustics*, 1990, 112: 2-7.

[10] Chen,J., Huang,Z., Bai,S. and Liu,Y., Theoretical analysis on the local critical stress and size effect for interfacial debonding in particle reinforced rheological materials. *Acta Mechanica Solida Sinica*, 1999, 12: 1-8.

[11] Weisbrod,G. and Rittel,D., A method for dynamic fracture toughness determination using short beams. *International Journal of Fracture*, 2000, 104: 89-103.

[12] Freund,L.B., Dynamic Fracture Mechanics. Cambridge University Press, 1990.

[13] Kavaturu,M. and Shukla,A., Dynamic fracture criteria for crack growth along bimaterial interfaces. *Journal of Applied Mechanics*, 1998, 65: 293-299.

[14] Liechti,K.M. and Knauss,W.G., Crack propagation at material interfaces: II experiments on mode interaction. *Experimental Mechanics*, 1982, 22: 383-391.
[15] Lambros,J. and Rosakis,A.J., Development of a dynamic decohesion criteria for subsonic fracture of the interface between two dissimilar materials//Proceedings of the Royal Society, London, 1995, A451: 711-736.
[16] Homma,H., Shockey,D.A. and Murayama,Y., Response of cracks in structural materials to short pulse loads. *Journal of the Mechanics and Physics of Solids*, 1983, 31: 261-279.
[17] Kalthoff,J.F. and Shockey.D.A., Instability of cracks under impulse loads. *Journal of Applied Physics*, 1977, 48: 986-993.
[18] Shockey,D.A., Kalthoff,J.F. and Erlich,D.C., Evaluation of dynamic crack instability criteria. *International Journal of Fracture*, 1983, 22: 217-229.
[19] Shockey,D.A., Erlich,D.C., Kalthoff,J.F. and Homma,H., Short-pulse fracture mechanics. *Engineering Fracture Mechanics*, 1986, 23: 311-319.
[20] Liu,C., Knauss,W.G. and Rosakis,A.J., Loading rates and the dynamic initiation toughness in brittle solids. *International Journal of Fracture*, 1998, 90: 103-118.
[21] Hearn,E.J., Mechanics of Materials, 2nd Edition. Pergamon Press, 1985.
[22] Chen,Z. and Yu,S., Anti-plane crack moving along the interface of dissimilar piezoelectric materials. *Acta Mechanica Solida Sinica*, 1999, 12: 31-35.
[23] Tada,H., Paris,P. and Irwin,G., The Stress Analysis of Cracks Handbook. Hellertown, Pennsylvania: Del Research Corporation, 1973.
[24] Hughes,T.J.R., The Finite Element Method: Linear Static and Dynamic Finite Element Analysis. Englewood Cliffs, New Jersey: Prentice-Hall, 1987.

APPENDIX I: CUT-ON *v.s.* CUT-OFF MODES

In §2.2, it is shown that three possible solution forms exist for the mode shape ψ_1, depending on the sign of the quantity $\lambda = \dfrac{k - m\Omega^2}{EI}$. Case 1 ($\lambda > 0$) gives the traditional solution form associated with a foundationless beam. This is an acceptable solution. Case 2 ($\lambda < 0$) and Case 3 ($\lambda = 0$) lead to unacceptable solutions. To see this, first consider the Case 2. The eigenvalue problem for a finite beam resting on an elastic foundation is

$$\psi_{xxxx} + \frac{k - m\Omega^2}{EI}\psi = 0$$

where ψ is the mode shape. Letting $\lambda = \dfrac{k - m\Omega^2}{EI}$, the above equation is multiplied by ψ and integrated over the domain:

$$\int_0^L \psi\psi_{xxxx}\mathrm{d}x - \lambda\int_0^L \psi^2\mathrm{d}x = 0$$

Integrating the first term by parts twice and applying the appropriate boundary conditions, this expression becomes

$$\int_0^L \psi_{xx}^2\mathrm{d}x - \lambda\int_0^L \psi^2\mathrm{d}x = 0$$

Both of the integrals are positive and, as a result, there is no negative value of λ that can satisfy this equation. So $\lambda < 0$ is not acceptable and Case 2 is eliminated as a possibility.

Finally, Case 3 is the cut-off case, $\lambda = 0$. Based on the above equation, ψ must satisfy $\psi_{,xx} = 0$ in the whole domain. This gives $\psi(x) = A_3x + A_4$, which is a rigid body motion. A_3x is the rotation and A_4 is the translation. But this deflection shape can not satisfy the geometric boundary conditions for a cantilever and, hence, Case 3 is not a possibility, either.

As shown, only Case 1 leads to an acceptable solution to the characteristic equation for a finite beam on an elastic foundation; this justifies the solution used in §2.2.

APPENDIX II: ORTHOGONALITY OF MODE SHAPES

To ensure the orthogonality of the mode shapes of a beam on a partial elastic foundation, the problem must be shown to be self-adjoint. To accomplish this, Eqs.(9) and (10) may be expressed as

$$\begin{aligned} &\psi^{\mathrm{I}}_{xxxx} + \lambda_1\psi^{\mathrm{I}} = 0 \qquad && (x < d) \\ &\psi^{\mathrm{II}}_{xxxx} + \lambda_2\psi^{\mathrm{II}} = 0 \qquad && (d \le x < L) \end{aligned}$$

where $\lambda_1 = \dfrac{-m\Omega^2 + k}{EI}$ and $\lambda_2 = \dfrac{-m\Omega^2}{EI}$. The eight boundary/matching conditions associated with this eigenvalue problem are stated in §2.1. The operator for these two equations is $L_i[\circ] = \dfrac{\partial^4 \circ}{\partial x^4} + \lambda_i \circ$, $i = 1, 2$. Now, consider two composite functions, f and g, which satisfy the boundary/matching conditions:

$$f = \begin{cases} f_1 & (x < d) \\ f_2 & (d \le x < L) \end{cases} \qquad \text{and} \qquad g = \begin{cases} g_1 & (x < d) \\ g_2 & (d \le x < L) \end{cases}$$

Self-adjointedness is, by definition, assured if $< L[f],\, g >=< f,\, L[g] >$. $< \circ >$ is an inner product operator over the whole domain defined as follows. The left hand side of this expression may be expressed as

$$\begin{aligned} < L[f],\, g > &= \int_0^d L_1[f_1] g_1 \mathrm{d}x + \int_d^L L_2[f_2] g_2 \mathrm{d}x \\ &= \int_0^d \frac{\partial^4 f_1}{\partial x^4} g_1 \mathrm{d}x + \int_0^d \lambda_1 f_1 g_1 \mathrm{d}x + \int_d^L \frac{\partial^4 f_2}{\partial x^4} g_2 \mathrm{d}x + \int_d^L \lambda_2 f_2 g_2 \mathrm{d}x \end{aligned}$$

Integrating the first and third terms by parts four times and applying the boundary/matching conditions of Eq.(8) yields:

$$< L[f], g >= \int_0^d \frac{\partial^4 g_1}{\partial x^4} f_1 \mathrm{d}x + \int_0^d \lambda_1 f_1 g_1 \mathrm{d}x + \int_d^L \frac{\partial^4 g_2}{\partial x^4} f_2 \mathrm{d}x + \int_d^L \lambda_2 f_2 g_2 \mathrm{d}x$$

The right hand side is simply $< f, L[g] >$. Hence, the system is self-adjoint.

APPENDIX III: DERIVATION OF EQUATION (17)

Substitute $w(x,t) = \sum_{j=1}^N \phi_j(t)\psi_j(x)$ into Eq.(16), times $\psi_i(x)$ and integrate from 0 to L

$$\begin{aligned} &\int_0^L \psi_i \left\{ m \sum_{j=1}^N \phi_{j,tt}\psi_j + c \sum_{j=1}^N \phi_{j,t}\psi_j + EI \sum_{j=1}^N \phi_j \psi_{j,xxxx} + k[1 - H(x-d)] \sum_{j=1}^N \phi_j \psi_j \right\} \mathrm{d}x \\ &\quad = \int_0^L P_o \sin(\omega t)\delta(x - L)\mathrm{d}x \end{aligned}$$

By applying the orthogonality of mode $\psi_j(x)$ to the left side terms and the Dirac delta function integration property to the right side term, the following equation is obtained

$$\int_0^L \psi_j^2 (m\phi_{j,tt} + c\phi_{j,t})\mathrm{d}x + \int_0^L \{\psi_j \psi_{j,xxxx} EI \phi_j + \psi_j^2 k[1 - H(x-d)]\phi_j\}\mathrm{d}x = P_o \sin(\omega t)\psi_j^{\mathrm{II}}(L)$$

By using Eqs. (6) and (7), the above equation can also be written as follows

$$\begin{aligned} &\int_0^L \psi_j^2 (m\phi_{j,tt} + c\phi_{j,t})\mathrm{d}x + EI\phi_j \left(\int_0^d \psi_j^{\mathrm{I}} \frac{m\Omega^2 - k}{EI} \psi_j^{\mathrm{I}} \mathrm{d}x + \int_d^L \psi_j^{\mathrm{II}} \frac{m\Omega^2}{EI} \psi_j^{\mathrm{II}} \mathrm{d}x \right) + k \int_0^d \psi_j^{\mathrm{I}} \psi_j^{\mathrm{I}} \mathrm{d}x \\ &\quad = P_o \sin(\omega t)\psi_j^{\mathrm{II}}(L) \end{aligned}$$

Grouping the terms of the above equation, the following equation is derived

$$\int_0^L \psi_j^2 (m\phi_{j,tt} + c\phi_{j,t})\mathrm{d}x + m\Omega^2 \phi_j \int_0^L \psi_j^2 \mathrm{d}x = P_o \sin(\omega t)\psi_j^{\mathrm{II}}(L)$$

When the above equation is divided by $m\int_0^L \psi_j^2 \mathrm{d}x$, Eq.(17) is derived.